Full-scale 3D remote sensing of wake turbulence - A taster

Larsen, Gunner Chr.; Pedersen, A. T.; Hansen, Kurt Schaldemose; Larsen, Torben J.; Courtney, Michael; Sjöholm, Mikael

Published in:
Proceedings of the Wake Conference 2019

Link to article, DOI:
10.1088/1742-6596/1256/1/012001

Publication date:
2019

Document Version
Publisher's PDF, also known as Version of record

Full-scale 3D remote sensing of wake turbulence - a taster

IOP Conf. Series: Journal of Physics: Conf. Series **1256** (2019) 012001 doi:10.1088/1742-6596/1256/1/012001

Full-scale 3D remote sensing of wake turbulence - a taster

G.C. Larsen, A.T. Pedersen, K.S. Hansen, T.J. Larsen, M. Courtney, M. Sjöholm

Technical University of Denmark, Department of Wind Energy
E-mail: gula@dtu.dk

Abstract. The aim of the present paper is to investigate the *wake turbulence* as based on advanced full-scale measurements which, for the first time, makes it possible directly to resolve all *three turbulence components* in the wake behind an operating wind turbine with high spatial- and temporal resolution. The experimental setup will be described, and analysis of selected runs will be presented with a focus on the expected *inhomogeneity* of this turbulence field. The analyses are performed in a *meandering frame* of reference, and in addition to afore mentioned wake turbulence field, the wake deficit field will be resolved and analysed. Atmospheric stability is not considered but is, however, not expected to contribute noticeably to wake turbulence nor to the wake deficit field when expressed in the meandering frame of reference.

1. Introduction

The dynamic wake meandering (DWM) model [1] - now included as a recommended practice in the IEC code [2] to describe flow fields in wind farms - is built on 3 corner stones: 1) a wake deficit; 2) a stochastic model for wake meandering; and 3) a description of the wake-generated small-scale turbulence. The aim of the present paper is to examine the third element in more detail based on advanced full-scale measurements which, for the first time, make it possible directly to resolve all three turbulence components (u, v, w) in the wake behind an operating turbine with high spatial- and temporal resolution. The wake generated turbulence has previously been investigated both numerically [3], [4], [5] and experimentally [6], [7], [8], [9] but, except for a single numerical study [3], the focus has up to now been only on the longitudinal turbulence component, u, or alternatively line of sight (LOS) turbulence components resulting from projecting the turbulence field on the LOS direction.

The paper is structured as follows: First the experimental setup is described in Section 2. Next follows results from a selected 10-minute case in Section 3, which is followed by a discussion of these in Section 4. Finally, conclusions are drawn in Section 5.

2. Experimental setup

The experimental campaign was conducted at the DTU Risø campus test site, where the flow field behind a V52 wind turbine was recorded using three synchronized continuous-wave Doppler lidars; i.e. the DTU short-range WindScanners [10]. These were simultaneously operated in a coordinated manner to resolve full 3D velocity vectors in this wake affected turbulent flow field along pre-defined scan patterns in a downstream vertical cross section perpendicular to the prevailing mean wind direction at the location.

2.1. Topology of the lidar triple set

The three Windscanner units - SRWS1, SRWS2 and SRWS3 - were each installed approximately 73m from the origo of the a priori defined measurement coordinate system with an angular separation of

around 120°. The elevation angle of the laser beams were set to about 30° from horizontal. The lidar setup was supplemented by a meteorological mast (denoted as '52 mast' in Figure 1) erected in the scan-plane and equipped with a sonic anemometer at 10m above ground level (a.g.l.) to facilitate reference wind speed and direction recordings as well as atmospheric boundary layer (ABL) stability classification. The experimental layout is illustrated in Figure 1.

Figure 1: Position of the three short-range WindScanners and the reference meteorological mast located east to the V52 turbine (left). The red line symbolizes the lidar scan plane.

2.2. Scan patterns

The requested (u, v, w) turbulence field is resolved along a predefined 'butterfly-shaped' trajectory in the selected downstream cross section. The lateral extension is approximately ±70m as measured from the origo of the measurement frame of reference, whereas the vertical extension is from ground level to approximately 90m a.g.l. at origo. To minimize the time it takes to complete a full scan, the beams will, after completing the vertical scan, move directly to the beginning of the horizontal part and vice versa. The defined scan pattern is shown in Figure 2.

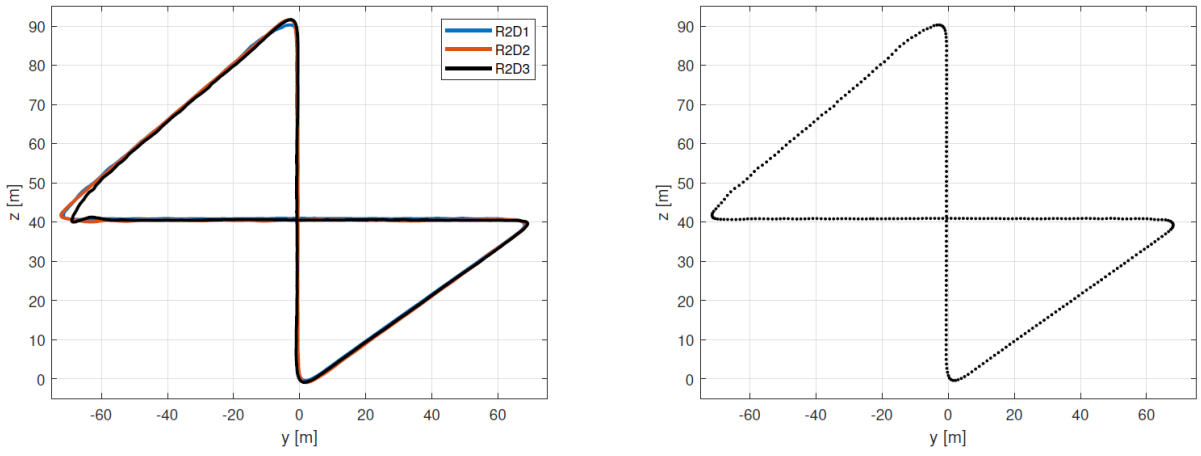

Figure 2: 'Coinciding' scan patterns of the three short-range WindScanners (left) and spatial resolution of the scan patterns (right).

The scan time of a full trajectory is approximately 1s and data is obtained at a rate of 322Hz meaning that the coordinated beam foci move about 1.2m during each sampling period. The sampling volume of each lidar beam depends on the position in the scan pattern as the distance to the lidars changes, and it

ranges from about 6m to 16m along the vertical scan line and from 1m to 24m along the horizontal line with the extreme values occurring at the extremes of the pattern.

3. Results

Following a convenient split in scales introduced in [1] and validated in [11], [12], [13] to separate wake dynamics from quasi-steady wake expansion and attenuation, we conduct the analysis of the wake deficit and the wake turbulence profiles in the *meandering frame of reference* (MFoR) - i.e. the frame following the stochastic meandering of the wake deficit at a given downstream distance and with the wake center located in origo. In principle meandering is taking place in both the lateral- and vertical directions. However, only the lateral wake dynamics are accounted for in the present analysis. This is because a full 2D wake centre tracking (i.e. laterally as well as vertically) is only possible with a fully 2D resolved cross section, and in this experiment only one vertical 'line' and one horizontal 'line' of lidar measurements are available (cf. Figure 2). Moreover, due to the design of the experiment with all three lidar's placed on the ground, the vertical velocity component cannot be resolved in the lower approximately 16.4m of the scan plane as will be detailed in Section 3.2. Restricting the MFoR to account only for lateral wake dynamics is thus a necessity following from the experimental setup, but can to some degree be justified by the more modest dynamics in the vertical direction compared to the lateral direction.

With the lidar recordings transformed to the meandering frame of reference, suitable temporal averaging yields the *mean* wake deficit field as well as the associated *variance*, from which the requested profiles may be derived.

3.1. Identification of MFoR

To facilitate a coordinate transformation from the fixed meteorological coordinate system (FFoR), in which the measurements are performed, to the MFoR, the instantaneous position of the wake deficit in the lateral direction is identified using a *least square* approach, which involves an assumed *generic wake deficit* shape. The identification of the wake position in all available lidar sweeps directly defines the meandering frame of reference.

Close to the rotor plane real wakes have a *bimodal shape* reflecting the radial dependence of the rotor thrust - at longer downstream distances turbulence diffusion erode this bimodal shape characteristics, and the wake gradually become more and more 'Gaussian-like'. In a horizontal cross section 40.6m a.g.l. in the scanning plane, the generic wake shape may be described by the sum of two Gaussian shapes with identical variance, since each of the 'wake modes' originates from identical average (i.e. excluding contributions from turbulence) rotor thrust conditions. Thus, the generic wake deficit, Δu, is defined as

$$\Delta u(y|A, y_c, \sigma, d) = A\left\{\mathrm{Exp}\left[-\frac{(y-y_c-d)^2}{2\sigma^2}\right] + \mathrm{Exp}\left[-\frac{(y-y_c+d)^2}{2\sigma^2}\right]\right\} \quad (1)$$

where y is the lateral coordinate, A is a wake deficit amplitude accounting for the fact that the integral over the wake deficit does in general not equal one as for the Gaussian probability density function, y_c is the (instantaneous) centre of gravity of the bimodal generic wake deficit, σ defines the width of the shape modes, and d is half the lateral distance between the shape modes.

To estimate the shape parameters for each lidar sweep we perform a χ^2-fit minimizing the sum of squared differences between the measured deficit (including turbulence contributions) and the generic wake deficit expressed in equation (1). The temporal development of y_c thereby defines the temporal location of origo of the MFoR relative to the meteorological coordinate system.

At sufficient long downstream distances, the generic wake deficit expressed in equation (1) degenerates to

$$\Delta u(y|A, y_c, \sigma) = 2A\left\{\mathrm{Exp}\left[-\frac{(y-y_c)^2}{\sigma^2}\right]\right\} \quad (2)$$

i.e. a Gaussian shape emerging from the parameter d being equal to zero in equation (1).

For the transformation from FFoR to MFoR a 'step-wise' Galilei transformation may be applied, which modify the lateral velocity components according to

$$v_j^{MFoR} = -\frac{\Delta y_j}{\Delta t_j} + v_j^{FFoR} \tag{3}$$

in which Δy_j is the identified lateral displacement of the wake deficit during the j'th time step Δt_j , and upper indices indicate type of coordinate system. Because the u- and w-turbulence components are perpendicular to the coordinate displacement, these are unaffected by the Galilei transformation.

To avoid introduction of spurious high-frequency v_i^{MFOR} contributions, caused by uncertainties in the estimation of the lateral position of the wake deficit and thus in turn in $\Delta y_i/\Delta t_i$, we have applied a low-pass Fourier filter to remove all lateral meandering fluctuations with frequencies above $U/(2D)$ [1], where U is the mean wind speed at hub height, and D is the rotor diameter (52m) of the wake generating rotor. The discrete estimated instantaneous wake positions at time t_j is thus initially represented as

$$y(t_j) = \sum_{k=0}^{N-1} c_k e^{i2\pi k t_j/T}\ ;\ c_k = \frac{1}{T}\sum_{j=0}^{N-1} y(t_j) e^{-i2\pi k t_j/T} \tag{4}$$

The requested filtering is next obtained by truncating the expansion defined in equation (4) in accordance with the cut-off condition $U/2D \geq 2\pi k/T$. Thus

$$y(t_j) = \sum_{k=0}^{N_t} c_k e^{i2\pi k t_j/T} \tag{5}$$

where $N_t = Trunc[UT/(4\pi D)]$, and $Trunc[*]$ denotes the truncation operator. The discrete wake lateral meandering velocity, $v(j)$, thereby has the following analytical representation

$$v(t_j) = \left.\frac{dy(t)}{dt}\right|_{t=t_j} = i2\pi/T \sum_{k=0}^{N_t} k c_k e^{i2\pi k t_j/T} \tag{6}$$

It is noted, that removal of spurious high-frequency v_i^{MFOR} contributions is especially important for variance and spectral analyses, whereas mean wake profiles, due to the averaging, is less sensitive.

3.2. Vertical cross sections of wake deficit and turbulence standard deviation

In this paper we focus on one particular 10-minute time period recorded 22-10-2018 in the time span 8:40-8:50. Simultaneously with the lidar recordings, the ambient mean wind speed shear was recorded at a nearby meteorological tower in 5 heights ranging from 18m to 70m above the terrain surface. Based on these recordings the mean wind speed shear was fitted to a power-law as defined in equation (7) below

$$U(z) = U(z_r)\left(\frac{z}{z_r}\right)^{\alpha} \tag{7}$$

where $U(z)$ is the mean wind speed at height z, α is the shear exponent, and z_r is some chosen reference height. Using the meteorological wind speed data from the investigated 10-minute period, the shear exponent was estimated to $\alpha = 0.05$. The resulting shear model is subsequently used to eliminate the shear contribution to the mean wind profile in the mean wind direction; thus essentially 'isolating' the along wind component of the wake deficit.

A more detailed analysis of the vertical wind speed- and turbulence profiles revealed problems with the lower part of the resolved wind field; - i.e. the regime between 0m and approximately 16.4m above the terrain surface. Here, we observed an unrealistic scattered behaviour caused by the present experimental layout's very poor ability to resolve the w-component of the flow field close to the ground.

This is due to the fact, that all three lidar systems are positioned on the ground, whereby the vertical velocity component is impossible to resolve at ground level and encumbered with large uncertainty in the vicinity of the ground. To circumvent this problem, we resolve *only* the 2D (*u*,*v*)-field in the critical range between terrain surface and approximately 16.4m above the surface.

Figures 3-5 show the vertical wake deficit and wake turbulence profiles expressed in the FFoR for the *u*-, *v*- and *w*-velocity components, respectively. It is noted that the *w*-profile is only available for the flow regime above 16.4m for the reason described above.

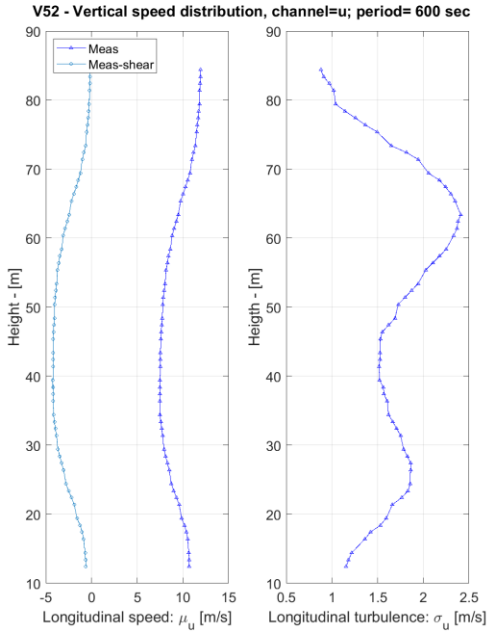

Figure 3. Vertical wake and turbulence profiles referring to the *u*-velocity component.

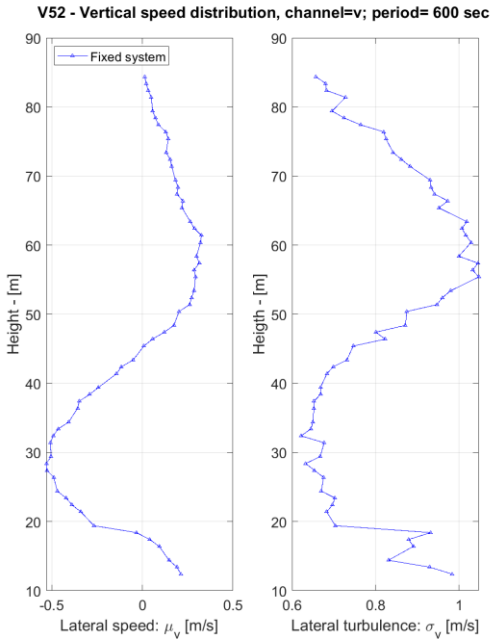

Figure 4. Vertical wake and turbulence profiles referring to the *v*-velocity component.

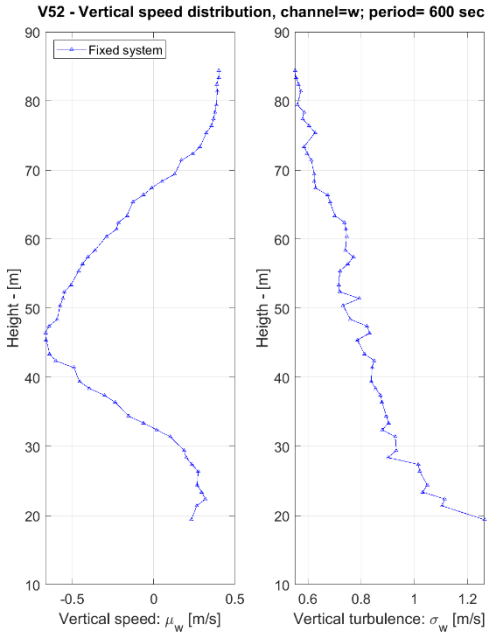

Figure 5. Vertical wake and turbulence profiles referring to the *w*-velocity component.

3.3. Lateral cross section of wake deficit and turbulence standard deviation

The lateral profiles of wake- and turbulence are resolved along a horizontal line located 40.6m above terrain in the FFoR as well as in the MFoR, and the results are shown in Figures 6-8 below.

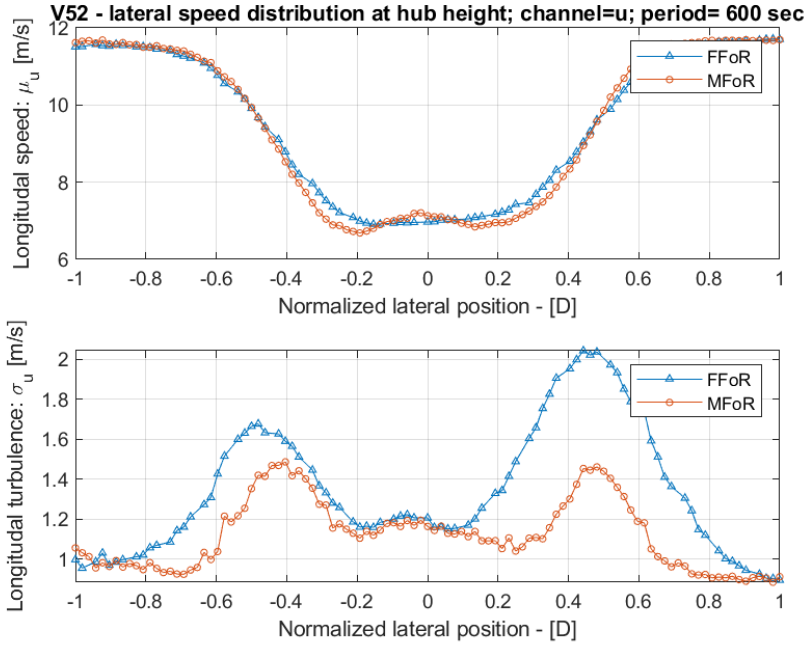

Figure 6. Horizontal wake and turbulence profiles referring to the *u*-velocity component.

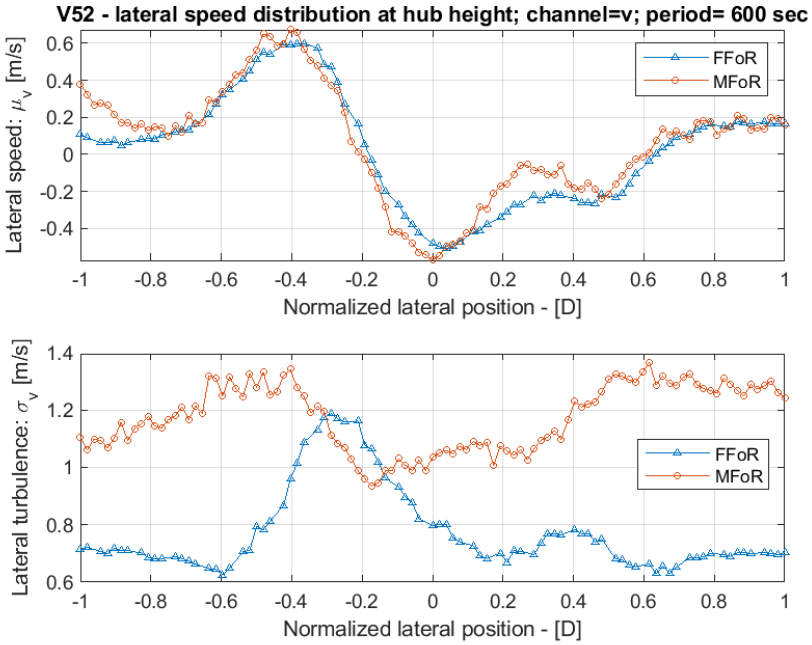

Figure 7. Horizontal wake and turbulence profiles referring to the *v*-velocity component.

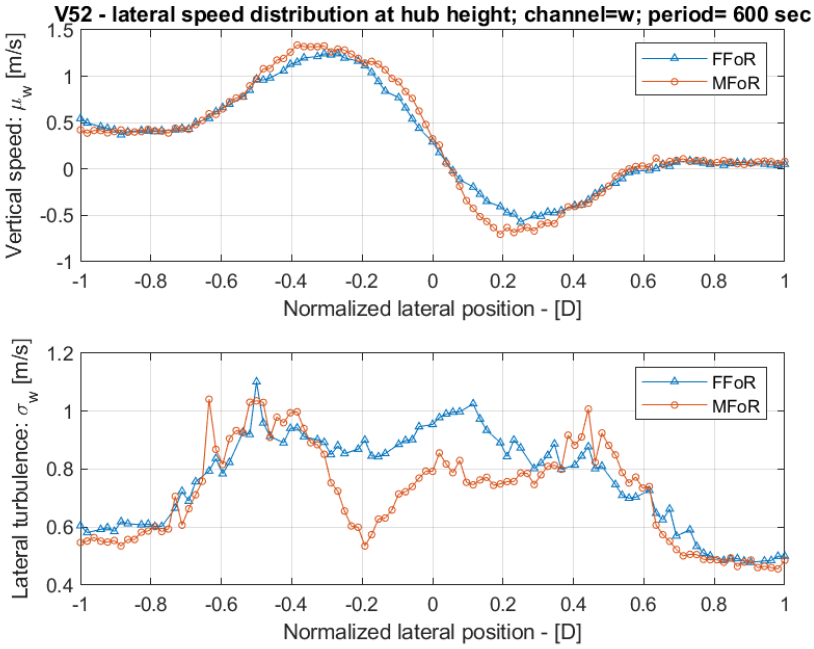

Figure 8. Horizontal wake and turbulence profiles referring to the *w*-velocity component.

3.4. Velocity spectra

In the wake affected flow regime, we have two sources of turbulence: 1) the ABL turbulence - including contributions from friction as well as buoyancy - and 2) the *wake induced turbulence* including contributions from conventional mechanically generated turbulence, caused by the wake shear, as well as from the rotor blade shed and trailed vortices mainly in terms of tip and root vortices gradually breaking down downstream of the wake generating rotor. These turbulence contributions are considered

statistically uncorrelated because of their independent origins, but naturally mixed together in the atmosphere and cannot be separated by analysis.

Thus, to investigate solely the wake generated turbulence based on full-scale measurements is clearly not a possibility, and only in case of very low ambient turbulence level this can be approximated. For the investigated time slot, the ambient turbulence intensity is of the order 9%, so, although not ideal, the best possible approach to analyse wake induced turbulence is to evaluate velocity spectra in spatial points with the largest possible share of wake induced turbulence - i.e. at the spatial points where the turbulence profiles are peaking (cf. Section 3.3), assuming that the ambient turbulence is reasonable horizontal homogeneous.

To eliminate the velocity variability associated with the wake deficit moving in and out of the observer point(s), we perform this analysis in the MFoR. Therefore, the focus is the on the two turbulence peaks observed in the lateral turbulence profiles. For reference purposes these are supplemented by spectra approximating ambient wind conditions - i.e. spectra associated with spatial locations outside the wake affected flow regime (r = 1.0D). For all spectra, the challenge is, that 10 minutes of measurements are indeed a modest amount of data for a frequency analysis. To obtain spectral estimates of satisfactory statistical significance, the resulting spectra were therefore (sequentially) block averaged with constant block length on a logarithmic scale. The results for the *u*, *v* and *w*-turbulence components are shown in Figures 9-11.

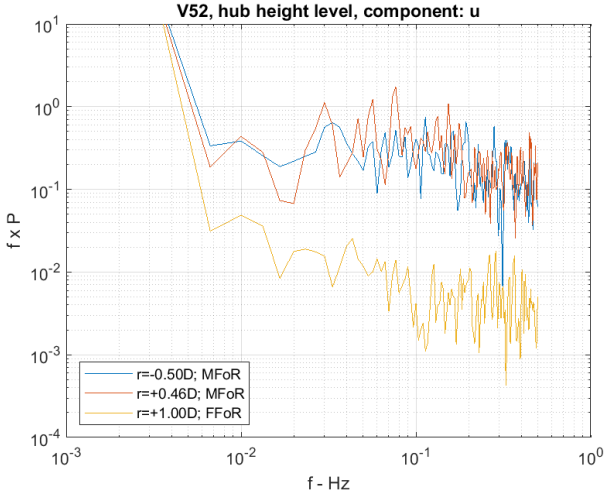

Figure 9. *u*-velocity spectra computed in the MFoR at turbulence intensity peaks (y = -22m, y = 24m).

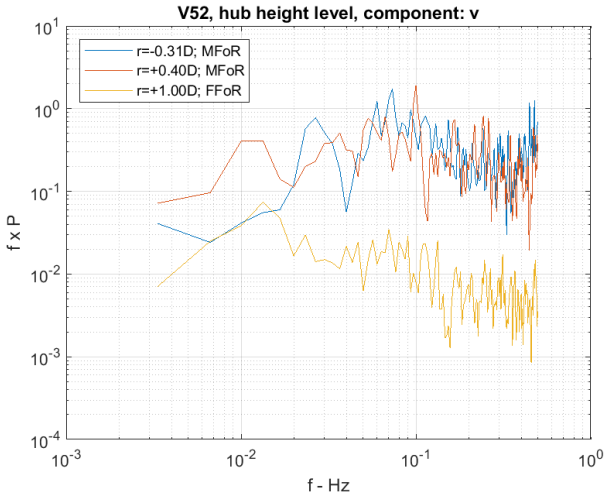

Figure 10. *v*-velocity spectra computed in the MFoR at turbulence intensity peaks (y = -22m, y = 24m).

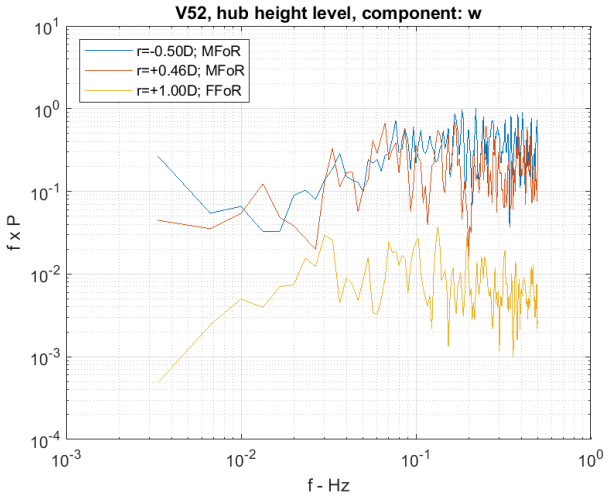

Figure 11. *w*-velocity spectra computed in the MFoR at turbulence intensity peaks ($y = -22$m, $y = 24$m).

4. Discussion

The discussion falls in two parts dealing with wake deficit and wake turbulence, respectively.

4.1. Wake deficit

Referring to Figures 3 and 6, the *extent* of the wake deficit in *horizontal* and *vertical* directions are seen to be close to identical and larger than the rotor diameter (i.e. 52m) due to mainly pressure recovery in the investigated near wake regime, and the wake profile is further *symmetric* around the wake centre when compensated for the mean wind speed shear. This agrees with previous findings in [6], where the investigated wake deficits were found to be approximately rotational symmetric. It is also observed, that the wake extend is slightly smaller when resolved in the MFoR compared to the FFoR, which is to be expected due to elimination of the meandering dynamics, and accordingly that the bi-modal wake shape is more pronounced with the wake resolved in the MFoR, because the averaging effect of wake meandering is eliminated. The wake deficit *magnitude* is, both measured along the horizontal line and the vertical line (after shear compensation), in the range 4-5m/s, which gives confidence to the measurements.

As for the *lateral* mean velocity component measured along the vertical line, *v*, it is interesting to note, that it is positive in the upper wake (wake) half-plane and negative in the lower (wake) half-plane (cf. Figure 4); thus indicating induced wake rotation which is contra-rotating the wake generating rotor as expected. It is, however, not 'pure' rotation but rather a mix of wake rotation and wake azimuthal deformation, since the lateral mean velocity component is not a linear function of the radial distance from the wake centre. The wake centre at the recorded downstream distance is approximately 45m a.g.l. if taken as the 'point' of rotation, and thus somewhat higher than the rotor centre at 40m a.g.l.. The reason might be terrain inclination upstream the wake generating turbine, but this needs more investigation.

Wake rotation is also observed in the *vertical* mean velocity component, *w*, measured along the horizontal line, where an almost anti-symmetric velocity profile is seen (cf. Figure 8). The two *w*-peaks are displace of the order of 0.6 rotor diameters, equal to 31m, and with magnitudes of the order of 0.7m/s. The distance between the two *v*-peaks measured along the vertical line is of the order of 33m and thus in practice identical to the distance between the *w*-peaks, described above, considering the measuring accuracy. The peak magnitudes, however, differs somewhat, as the *v*-peak magnitudes is of the order of 0.4m/s only. This again indicates some degree of azimuthal wake deformation.

Based on a rotational symmetry presumption, the mean wake *w*-component along the vertical line (cf. Figure 5) should correspond to the mean wake *v*-component along the horizontal line (cf. Figure 7).

This is not observed. The horizontal mean *v*-profile is anti-symmetric indicating an ongoing wake expansion, but the vertical mean *w*-profile is rather symmetric, thus indicating a continuing overall wake elevation combined with a radial wake distortion along this line.

4.2. Wake turbulence

ABL turbulence is usually well approximated with a homogeneous anisotropic turbulence field. These features are not found in wake induced turbulence fields, which appears to be pronounced *inhomogeneous* - cf. Figures 3-8. This is in accordance with results from both previous full-scale experiments resolving the *u*-turbulence component [6] and detailed CDF computations [4].

The *horizontal u*-turbulence profile clearly displays the expected two distinct peaks at locations corresponding to the maximum gradients of the wake deficit field projected on the along wind direction and thus symmetric around the wake centre. However, as mentioned in Section 3.4, the recorded turbulence fields contains contributions both from ABL turbulence and wake induced turbulence. If estimated from the flow regime outside the wake, the 'mean' (i.e. standard deviation) ABL turbulence contributions is of the order of 1m/s, which corresponds to a turbulence intensity of approximately 9% with a mean wind speed of approximately 11.5m/s at hub height. This is also what is found from the reference met. mast observations from the same time slot. With the previously argued uncorrelated characteristic of the two turbulence 'sources', the wake induced contribution can be estimated from

$$\sigma_{u,wake} = \sqrt{{\sigma_{u,tot}}^2 - {\sigma_{u,amb}}^2} \tag{8}$$

where $\sigma_{u,wake}$ is the wake-generated standard deviation of the *u* turbulence component, $\sigma_{u,tot}$ is the total standard deviation of the *u* turbulence component, and $\sigma_{u,amb}$ is the standard deviation of the *u* turbulence component originating from ambient ABL turbulence.

The *vertical u*-turbulence profile shows the characteristics with the same two distinct peaks, and the ambient ABL *u*-turbulence standard deviation is also for these recordings of the order of 1m/s.

For the *v*-turbulence profiles resolved in FFoR the same two peaks in turbulence standard deviation can be observed, however, with a smaller amplitude, which might reflect the reduced intensity of the ABL *u*- and *v*-turbulence. Estimated from Figure 7, the ABL *v*-turbulence contribution is of the order of 0.7m/s, thus consistent with the well-established ratio between *u*- and *v*-turbulence standard deviations for flat and homogeneous terrain (i.e. approximately 0.75). However, when resolved in the MFoR we see a contra-intuitive behaviour of the horizontal *v*-turbulence profile (although still with indications of turbulence peaks located symmetric around the wake centre), since the turbulence level is expected to decrease due to the inherent high pass filtering following the transformation from FFoR to MFoR. The opposite is observed, which must be ascribed inaccuracies introduced by the Galilei transformation (i.e. eq. (3)) despite the introduced filtering (cf. eq. (6)). The cut-off frequency (i.e. $U/(2D)$) of the high-pass filter can be of cause be disputed, and lowering the cut-off frequency will decrease the *v*-turbulence level expressed in the MFoR, compared to what is shown in Figure 7- although not beyond the turbulence level expressed in the FFoR, which is unexpected. A more symmetric turbulence profile is, however, resulting from the MFoR mapping compared to the FFoR representation, which is according to expectations. The decrease of *v*-turbulence level with decreasing cut-off frequency is followed by an increase of the *u*-turbulence level expressed in the MFoR, and the bi-modal behaviour of the *u*-deficit is at the same time less pronounced, thus indicating a less successful elimination of the meandering dynamics for lower cut-off frequencies than $U/(2D)$. The resolution of the *u*-turbulence in the MFoR is considered more 'robust' than the *v*-turbulence counterpart primary due to the uncertainty associated with the estimation of the gradient of the wake meandering dynamics (cf. eq. (3)), and therefore the conjectured cut-off frequency of $U/(2D)$ is retained throughout the present investigation. An explanation of the apparent inconsistency, resulting in counter acting effects on respectively *u*- and *v*-turbulence levels caused by the transformation from FFoR to MFoR, is at present unknown and left for future investigations.

The *w*-turbulence profile seems to decrease almost linearly with height (cf. Figure 5). Around the wake centre the standard deviation is of the order of 0.8m/s, which is also found in the horizontal profile (cf. Figure 8). The ambient *w*-turbulence level estimated from Figure 8, is again consistent with well-established results from flat and homogeneous terrains - i.e. $\sigma_w \approx 0.5\sigma_u$. A double peak structure, again symmetric around the wake centre, is observed in the horizontal profile when resolved in the MFoR (cf. Figure 8), but cannot be distinguished in the vertical profile.

The above *statistical* considerations on the wake induced turbulence can be extended to more detailed considerations on the *turbulence structure*, when investigating the turbulence velocity spectre presented in Section 3.4. As previously noted, the focus is on two points in space, which is characterized by their ability to represent the two turbulence intensity peaks identified in the *horizontal turbulence profile* in Figure 6. Although challenged regarding the *v*-turbulence component, the analysis is performed in the MFoR to isolate 'true' wake turbulence by eliminating velocity fluctuations caused by the wake deficit dynamics (i.e. spurious turbulence contributions). For this analysis the two points with y-coordinates respectively -22m and 24m have been chosen.

As an introductory remark, we note that the inherent lidar spatial averaging acts like a low pass filter for the investigated wind speed signals, whereas the transformation to the MFoR acts as a high pass filter, since the large meandering scales are eliminated with this transformation.

ABL turbulence - and turbulence in general (Kolmogorov '41) - is conventional subdivided in three spectral regimes: 1) the energy containing regime where turbulent energy is produced; 2) the inertial subrange, where energy neither produced or dissipated; and 3) the dissipation regime, where kinetic energy are transformed to heat. The *inertial subrange* regime is usually the ABL turbulence regime relevant for wind turbine loading, and characterized by the celebrated -5/3 power law. In a log-log representation of the spectra, the inertial subrange power law thus appears as spectra with a constant slope.

Referring to Figure 9, the -5/3 power law is clearly identified for the *u*-turbulence component in the frequency band extending from 0.1Hz to approximately 0.3Hz, beyond which the signal is dominated by (white) noise. Referring to Figures 10 and 11, the -5/3 regime is difficult to identify - or at the best limited to a narrow frequency band extending from 0.1Hz to 0.2Hz for the *v*-turbulence component and from 0.15Hz to 0.2Hz for the *w*-turbulence component. Beyond 0.2Hz the measurements are dominated by noise. Compared to the *v*- and *w*-spectra, the *u*-turbulence spectra display relative more energy on the largest scales, which may be an artefact of the MFoR not compensating for large ABL turbulence scales in the along wind direction, but also because of differences in turbulence length scales.

The spectral energy in the *u*-, *v*-, and *w* spectra at the investigated variance peaks in the MFoR are of the same order of magnitude (cf. eq. (8)), thus supporting an assumption of approximately *isotropic* wake generated turbulence. This assumption is inspired by previous numerical studies [15]. Assuming that the *wake generated* turbulence is approximately isotropic, the *u* length scale should be of the order 1.45 larger than the *v*- and *w* length scales [16], which in turn means that the *resolved* part of the *v*- and *w* spectra is relatively more dominated by energy containing regime than the *u*-spectrum. On top of this, it should be noted that the wake induced turbulence is confined to scales conjectured at least a decade smaller than ABL turbulence, meaning that the inertial subrange regime associated with this type of turbulence, compared to ABL turbulence, is relatively less important for wind turbine loading due to aerodynamic admittance.

5. Conclusion

For the first time an advanced lidar technology has been used to resolve all *three velocity components* in the wake behind an operating wind turbine with high spatial- and temporal resolution. Temporal and spatial resolution need to be balanced, and the selected scan pattern therefore mainly resolve the wake affected flow field along a horizontal and a vertical line in a downstream cross section. Based on the recordings, the 3D mean velocity wake deficit is resolved and subsequently used to analyse the associated 3D wake affected turbulence field.

The mean velocity deficit is, along the resolved lines, shown to be symmetric. Further the wake deficit flow structure are shown rotate as a consequence of the rotor azimuthal induction.

The wake induced turbulence is seen to be clearly *inhomogeneous*. As it cannot be completely separated from the ambient ABL turbulence, it is a challenge to analyse in detail the turbulence structure of wake induced turbulence as based on full-scale measurements. However, focusing on spatial points with a high share of wake turbulence some general indications can be found. These are that the wake turbulence seems predominantly *isotropic*, and that it, regarding the *resolved* part of the *v*- and *w* spectra resulting from the present measurements, mainly resembles the characteristics an *energy containing spectral regime* rather than an inertial subrange regime.

In a future perspective, more data will be analysed - in the first place to consolidate the present spectral investigations, where the present analysis of only one 10-minute time series is absolutely in the low end - and later with particular focus on low wind speed events under stable stratification, such that the undesirable influence from ABL turbulence is reduced to the largest possible extent. It is here noted, that the ABL stability condition is not expected to affect the wake generated small-scale turbulence notably [17], [18]. As part of these future additional analyses, a critical view on the apparent inconsistent effect on the *v*-turbulence component, caused by the Galilei transformation from FFoR to MFoR, will be included.

References

[1] Larsen GC, Madsen HAa, Thomsen K and Larsen TJ (2008). Wake meandering - a pragmatic approach. Wind Energy, **11**, pp. 377–395.
[2] IEC 61400-1:2019, Wind energy generation systems - Part 1: Design requirements.
[3] Larsen GC et al. (2008). Wake modeling and simulation. Risø-R-1653(EN
[4] Larsen GC, Hansen KS, Troldborg N, Mann J, Enevoldsen K and Bingöl J (2010). An attempt to characterize the Structure of Wake Turbulence using a combined Experimental and Numerical Approach. iTi conference on turbulence, Springer Proceedings in Physics 141.
[5] van der Laan MP and Andersen SJ (2018). The turbulence scales of a wind turbine wake: A revisit of extended k-epsilon models *J. Phys.: Conf. Ser.* **1037** 072001.
[6] Larsen GC, Hansen KS, Mann J, Bingöl F and Enevoldsen K (2010). Full scale measurements of wind turbine wake turbulence. In *The Science of making Torque from Wind*, Heraklion, Crete, Greece.
[7] Iungo GV,GO, Wu Y-T and Porté-Agel F (2013). Field Measurements of Wind Turbine Wakes with Lidars. Journal of Atmospheric and Oceanic Technology, vol. 30.
[8] Espanã G, Aubrun S, Loyer S, and Devinant P (2012). Wind tunnel study of the wake meandering downstream of a modelled wind turbine as an effect of large scale turbulent eddies. Journal of Wind Engineering and Industrial Aerodynamics, **101**, 24–33.
[9] Wittwer AR, Dorado R, Alvarez GA, Degrazia GA, Loredo-Souza AM and Bodmann B (2016). Flow in the Wake of Wind Turbines: Turbulence Spectral Analysis by Wind Tunnel Tests. American Journal of Environmental Engineering 2016, 6(4A): 109-115.
[10] Simley E, Angelou N, Mikkelsen M, Sjöholm M, Mann J and Pao LY (2016). Characterization of wind velocities in the upstream induction zone of a wind turbine using scanning continuous-wave lidars. Journal of Renewable and Sustainable Energy, **8**, 013301.
[11] Bingöl F, Mann J, Larsen GC (2010). Light detection and ranging measurements of wake dynamics. Part I: one-dimensional scanning. Wind Energy, **13**(1), pp. 51–61.
[12] España G, Aubrun S, Loyer S, Devinant P. (2012). Wind tunnel study of the wake meandering downstream of a modeled wind turbine as an effect of large scale turbulent eddies. Journal of Wind Engineering and Industrial Aerodynamics, **101**, pp. 24–33.
[13] Machefaux E, Larsen GC, Troldborg N, Gaunaa M and Rettenmeier A. (2015). Empirical modeling of single-wake advection and expansion using full-scale pulsed lidar-based measurements. Wind Energy, **18**, pp. 2085–2103.

[14] Madsen HAa, Larsen GC, Larsen TJ, Troldborg N. (2010). Calibration and validation of the dynamic wake meandering model for implementation in an aeroelastic code. Journal of Solar Energy Engineering 2010; **132**(4): 041014 (14 pages).
[15] Larsen GC et al. (2007). Dynamic wake modeling, Risø-R-1607(EN), Risoe National Laboratory, Technical University of Denmark.
[16] Mann, J. (1994). The Spatial Structure of Neutral Atmospheric Surface-Layer Turbulence. J. of Fluid Mech., 273, pp. 141-168.
[17] Larsen GC, Machefaux E and Chougule A (2015). Wake meandering under non-neutral atmospheric stability conditions – theory and facts. Journal of Physics: Conference Series (Online), 625, 012036.
[18] Machefaux E, Larsen GC, Tilman K, Troldborg N, Kelly MC, Chougule A, Hansen KS and Rodrigo KS (2016). An experimental and numerical study of the atmospheric stability impact on wind turbine wakes. Wind Energy, **19**, pp. 1785–1805.